Electron beam melting of H13 tool steel: parameter optimization, microstructure and mechanical properties

Jia-qi Deng1, Geng-jie Wang1, Yong-xin Jian1, *Zhi-fu Huang1
1. State Key Laboratory for Mechanical Behavior of Materials, School of Materials Science and Engineering, Xi'an Jiaotong University, Xi'an, 710049, China
*Corresponding address: e-mail: hzf@mail.xjtu.edu.cn

Abstract: This study investigates the fabrication of H13 tool steel using electron beam melting (EBM) technology, focusing on the optimization of processing parameters and their influence on microstructure and mechanical properties. Beam current and scanning speed were systematically varied to optimize the consolidation quality. Microstructural characterization revealed that specimens fabricated under optimal conditions exhibited a refined martensitic-bainitic dual-phase structure, with high-density dislocations and nanoscale carbides. X-ray diffraction (XRD) confirmed the dominant ferrite with minimal retained austenite. The optimized samples achieved a relative density exceeding 99.5%, an ultimate tensile strength of 1780 MPa, a yield strength of 1335 MPa, and an elongation of approximately 10.5%. Strengthening mechanisms including grain boundary strengthening, dislocation strengthening, and precipitation strengthening were quantitatively analyzed, and theoretical calculations showed good agreement with experimental results. These findings demonstrate that careful optimization of EBM parameters can significantly improve the mechanical performance of H13 steel by tailoring its microstructure, providing valuable guidance for the additive manufacturing of high-performance tooling materials.
Keywords: Electron beam melting; H13 tool steel; Microstructure; Mechanical properties; Strengthening mechanisms

1 Introduction

H13 tool steel, characterized by its excellent thermal stability, high strength, and wear resistance, is widely utilized in tooling, die-making, and other demanding industrial applications that require materials to sustain high temperatures and mechanical stresses [1-4]. With the growing demand for complex and high-performance components, Additive manufacturing (AM) has emerged as a promising technology due to its ability to produce near-net-shape parts with reduced material waste and high processing efficiency [5-7]. Electron beam melting (EBM), as one of the most prevalent AM techniques, offers unique advantages in processing high-performance metallic components [8-11]. By utilizing a high energy electron beam in vacuum environment, EBM ensures precise thermal control for uniform melting while protecting parts from potential contamination. Additionally, EBM technology enables control over processing temperature, reaching up to 1100 ℃, which reduces residual stress generated during fabrication [12, 13]. As a result, EBM offers a competitive alternative to traditional manufacturing methods like casting and forging. Despite its potential, achieving optimal mechanical performance in EBM-fabricated H13 steel requires careful control and optimization of processing parameters due to their significant influence on microstructure and resultant mechanical properties [14-16]. This work aims to fill this gap by systematically investigating processing parameters, correlating them with microstructural evolution, and evaluating their effects on mechanical properties.

2 Experimental section

Plasma rotating electrode atomized H13 steel powder with an average particle size of 95 μm was used as the raw material, and its specific chemical composition is listed in Table 1. EBM fabrication was performed on a Y150 system under vacuum conditions (<5×10^{-3} Pa). Key parameters investigated were beam current (6–14 mA) and scanning speed (2000–5000 mm/s). The remaining parameters were maintained constant: voltage at 60 kV, hatch spacing at 50 μm, and layer thickness at 100 μm. As shown in Fig. 1, an extensive range of volumetric energy densities (VED) was investigated to achieve optimal microstructural and mechanical properties in EBM-processed H13 steel. VED was calculated using the formula VED = P/(v*h*t), where P is input power (P = U*I).

Table 1. Chemical composition of H13 steel powder (wt.%).

C	Si	V	Cr	Mn	Mo	Fe
0.41	0.93	0.95	5.37	0.35	1.16	Bal.

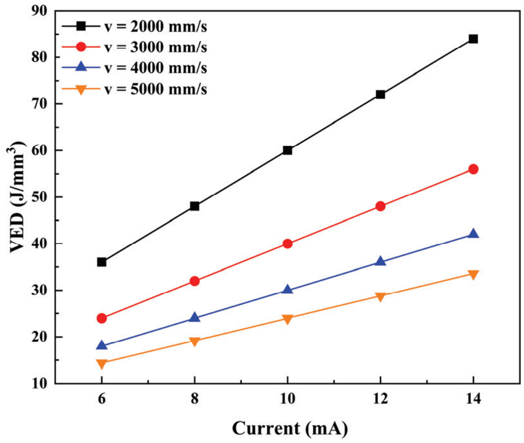

Fig. 1: Samples produced as a function of beam current and scanning speed and their respective VED.

Microstructural characterization was conducted using optical microscopy (OM), field-emission scanning electron microscopy (FE-SEM), and transmission electron microscopy (TEM). Phase composition analysis was performed using X-ray diffraction (XRD). The microstructural features such as grain size, grain boundary angle and texture were examined by electron backscattered diffraction (EBSD). Mechanical property evaluations included universal tensile testing conducted according to GB/T228.1-2010 standard.

3 Results and discussion

3.1 Processing parameter optimization

The relationship between processing parameters and relative density was systematically established through optical image analysis, as shown in Fig. 2. The results reveal that the VED plays a decisive role in determining the densification behavior of EBM-fabricated H13 steel. At lower beam currents (6–8 mA) or excessively high scanning speeds (4000–5000 mm/s), insufficient energy input led to poor powder melting and the formation of lack-of-fusion defects. Consequently, the relative density of the specimens remained below 98%. In contrast, increasing the beam current to 10–12 mA and employing moderate scanning speeds (2000–3000 mm/s) effectively promoted complete melting, resulting in a dense microstructure with relative densities exceeding 99.5%. However, further increasing the beam current beyond 12 mA caused localized over-melting, inducing defects such as keyhole porosity, which negatively impacted the relative density of the samples. Therefore, the optimal processing parameters were identified as 10 mA beam current combined with 3000 mm/s scan speed, where a balanced VED ensured full powder consolidation while effectively suppressing defect formation.

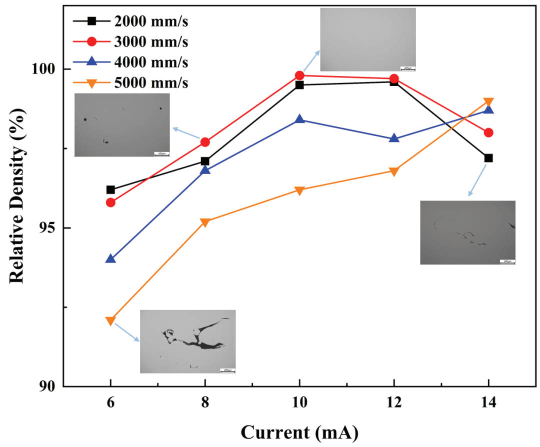

Fig. 2: Relationship between beam current, scanning speed, and relative density of EBM-fabricated H13 samples.

3.2 Microstructural analysis

XRD analysis (Fig. 3a) confirmed that the specimen fabricated under optimal processing conditions exhibited exclusively body-centered cubic (BCC) phase diffraction signatures, with no detectable peaks corresponding to the face-centered cubic (FCC) phase, demonstrating the absence or very low content of retained austenite. Detailed microstructural analysis was conducted on the specimen fabricated under the optimal parameters. SEM observations (Fig. 3b) reveal that the EBM-fabricated H13 sample exhibits a dual-phase microstructure comprising dark-etched martensitic regions and light-toned bainitic domains through differential etching response. EBSD results (Fig. 4) showed a refined grain structure with an average grain size of approximately 3.95 μm. A high proportion of high-angle grain boundaries (HAGBs, >15°) was detected, which effectively impede dislocation motion and improve both strength and toughness. Furthermore, Pole figures (PFs) shown in Fig. 4c demonstrate that the crystallographic texture is relatively weak, which is attributed to rapid solidification and random grain growth during the EBM process.

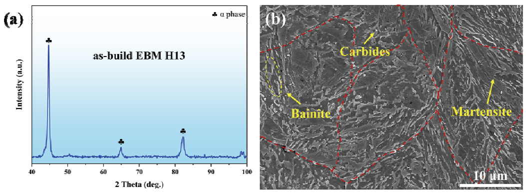

Fig. 3: (a) XRD pattern and (b) SEM image of H13 sample fabricated under optimal processing conditions.

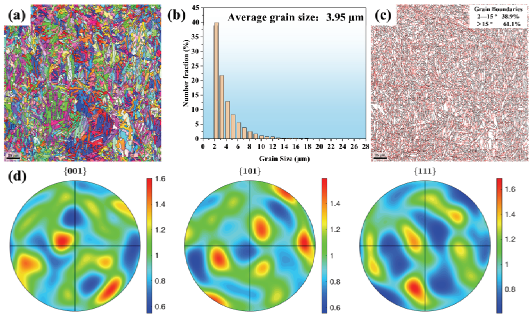

Fig. 4: The EBSD analysis of the optimally processed sample.

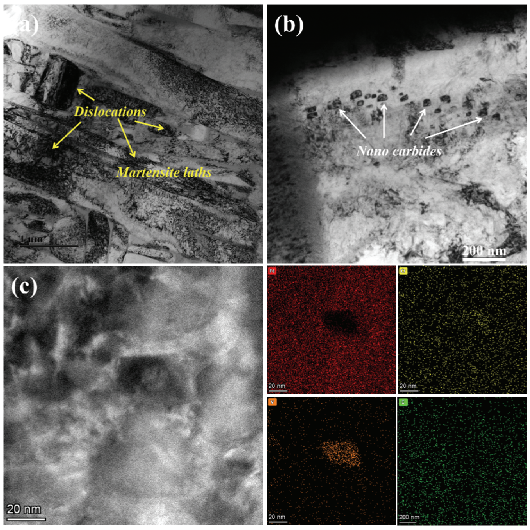

Fig. 5: TEM images showing the detailed microstructure of the optimally processed sample.

TEM analysis (Fig. 5) provided further insight into the nanoscale features. High-density dislocations were observed within the martensitic laths. Moreover, a large number of nanoscale V_8C_7 carbide precipitates were observed, providing additional barriers to dislocation motion during deformation and significantly enhancing the contribution of precipitation strengthening.

3.3 Mechanical properties

Fig. 6 shows the engineering tensile stress-strain curves and average results of the EBM-fabricated H13 sample at room temperature. The sample exhibited an ultimate tensile strength (UTS) of 1780 MPa and a yield strength (YS) of 1335 MPa, accompanied by an elongation to fracture of approximately 10.5%. Compared with conventionally processed H13 steel, the mechanical properties exhibit a remarkable enhancement, highlighting the critical role of the refined microstructure and the synergistic effect of the martensitic-bainitic mixed structure produced by the optimized EBM process.

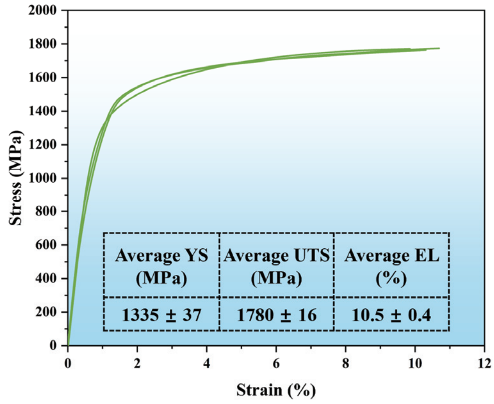

Fig. 6: Stress-strain curves and corresponding tensile data of the optimized samples.

The process parameters exerted significant effect on the mechanical property of EBM-fabricated H13 steels. It is well known that yield strength is governed by the synergistic effect of various microstructural features. In this work, the primary strengthening mechanisms include lattice friction (σ_0), grain boundary strengthening (σ_{gb}) from the refined martensitic-bainitic matrix, dislocation strengthening (σ_{dis}) due to high-density dislocations observed in TEM analysis, and precipitation strengthening (σ_p) contributed by nanoscale carbides. For simplicity, it can be expressed using the following equation [17]:

$$\sigma_y = \sigma_0 + \sigma_{gb} + \sigma_{dis} + \sigma_p \quad (1)$$

According to a previous study, the lattice friction stress of the H13 steel is 140 MPa.

The contribution of grain boundary strengthening can be estimated by the following:

$$\sigma_{gb} = kd^{-1/2} \quad (2)$$

where k is the Hall-Petch slope taken as 572 MPa $\mu m^{1/2}$ for the H13 steels [18], and d is the average grain size. As a consequence, the estimated value of σ_{gb} is 287.8 MPa.

The contribution of dislocation strengthening to the YS can be explained by the following formula:

$$\sigma_{dis} = \alpha MGb\rho^{1/2} \quad (3)$$

where α is an empirical constant, normally taken as 0.33 for BCC lattice, M is the Taylor factor counting for 3, G is the shear modulus of 70 GPa, b is the Burgers vector taken to be 0.25 nm [19], and ρ refers to the average value of the geometrically necessary dislocation (GND) density obtained from EBSD data. The contribution from dislocation strengthening to YS is evaluated as 542.2

MPa.

The precipitation strengthening caused by precipitates can be calculated by the Orowan bypass mechanism [20]:

$$\sigma_p = (0.538Gbf_i^{1/2}/r_i) \cdot \ln(r_i/2b) \quad (4)$$

where r_i is the average size of the precipitates and f_i is the volume fraction of the precipitates. According to TEM results, V_8C_7 carbides were identified in the SEBM H13 steels. The f and r of the V_8C_7 carbides in the sample are 2.32 % and 13.5 nm, taken from the TEM results in Fig. 5. As a result, the calculated σP is 350.1 MPa.

The calculated YS of the H13 sample fabricated under optimal processing conditions is approximately 1320.2 MPa. The theoretical prediction aligns well with the experimentally measured YS, validating the effectiveness of the strengthening mechanisms considered in this study.

4 Conclusions

In this study, the effects of electron beam melting (EBM) processing parameters on the microstructure and mechanical properties of H13 tool steel were systematically investigated. The main conclusions are as follows:

1.A beam current of 10 mA combined with a scanning speed of 3000 mm/s was identified as the optimal processing condition, achieving a dense microstructure with a relative density exceeding 99.5%. Excessively low or high volumetric energy densities led to lack-of-fusion defects or keyhole porosity, respectively.

2.The optimized EBM-fabricated H13 steel exhibited a refined dual-phase microstructure composed of martensitic and bainitic regions. The average grain size was approximately 3.95 μm, with a high fraction of high-angle grain boundaries (HAGBs). TEM observations confirmed the presence of a high density of dislocations and abundant nanoscale V_8C_7 carbide precipitates within the optimized sample.

3.The optimized sample achieved an ultimate tensile strength (UTS) of 1780 MPa, a yield strength (YS) of 1335 MPa, and an elongation to fracture of 10.5% at room temperature. Compared with conventionally processed H13 steel, the mechanical properties exhibited a remarkable improvement, mainly attributed to the synergistic effect of fine grain structures, high dislocation density, and precipitation strengthening.

Conflicts of interest:

The authors declare that they have no known competing financial interests or personal relationships that could have appeared to influence the work reported in this paper.

References

[1] J. Wang, S. Wang, W. Wu, D. Wang, J. Zhao, Z. Yang, H. Chen, Achieving ultrahigh yield strength and decent toughness in an in-situ alloyed H13 steel via laser powder bed fusion, Additive Manufacturing 85 (2024) 104169.

[2] H. Ding, Z. Yuan, T. Liu, L. Chen, Y. Zhou, Y. Cao, F. Cao, R. Luo, X. Cheng, Microstructure and high-temperature tensile behavior of modified H13 steel with the addition of tungsten, molybdenum, and lowering of chromium, Materials Science and Engineering: A 866 (2023) 144655.

[3] E.B. Fonseca, A.H.G. Gabriel, J.A. Ávila, R.F. Vaz, D.B. Valim, I.G. Cano, É.S.N. Lopes, Fracture toughness and wear resistance of heat-treated H13 tool steel processed by laser powder bed fusion, Additive Manufacturing 78 (2023) 103862.

[4] G.H. Zeng, T. Song, Y.H. Dai, H.P. Tang, M. Yan, 3D printed breathable mould steel: Small micrometer-sized, interconnected pores by creatively introducing foaming agent to additive manufacturing, Materials & Design 169 (2019) 107693.

[5] P. Bajaj, A. Hariharan, A. Kini, P. Kürnsteiner, D. Raabe, E.A. Jägle, Steels in additive manufacturing: A review of their microstructure and properties, Materials Science and Engineering: A 772 (2020) 138633.

[6] K. Li, T. Yang, N. Gong, J. Wu, X. Wu, D.Z. Zhang, L.E. Murr, Additive manufacturing of ultra-high strength steels: A review, J. Alloys Compd. 965 (2023) 171390.

[7] H. Cheng, X. Luo, X. Wu, Recent research progress on additive manufacturing of high-strength low-alloy steels: Focusing on the processing parameters, microstructures and properties, Materials Today Communications 36 (2023) 106616.

[8] C. Körner, Additive manufacturing of metallic components by selective electron beam melting - a review, Int. Mater. Rev. 61(5) (2016) 361-377.

[9] C. Ledford, P. Fernandez-Zelaia, T. Graening, Q. Campbell, J.O. Rojas, A.M. Rossy, Y. Kato, M.M. Kirka, Microstructure and high temperature properties of tungsten processed via electron beam melting additive manufacturing, International Journal of Refractory Metals and Hard Materials 113 (2023) 106148.

[10] Y. Li, W. Kan, Y. Zhang, M. Li, X. Liang, Y. Yu, F. Lin, Microstructure, mechanical properties and strengthening mechanisms of IN738LC alloy produced by Electron Beam Selective Melting, Additive Manufacturing 47 (2021) 102371.

[11] Y. Li, Y. Wang, J. Niu, S. Liu, Y. Lin, N. Liu, J. Ma, Z.

Zhang, J. Wang, Microstructure and mechanical properties of M2 high speed steel produced by electron beam melting, Materials Science and Engineering: A 862 (2023) 144327.

[12] X. Yang, F.-H. Wang, W.-L. Wang, S.-F. Liu, Y.-Q. Chen, H.-P. Tang, Comparison of two-step surface treatment on surface roughness and corrosion resistance of TC4 alloy parts prepared by SLM and SEBM, J. Alloys Compd. 921 (2022) 165929.

[13] Y. Shi, S. Gong, H. Xu, G. Yang, J. Qiao, Z. Wang, J. Zhang, B. Qi, Electron beam metal additive manufacturing: Defects formation and in-process control, Journal of Manufacturing Processes 101 (2023) 386-431.

[14] Y. Liu, C. Chen, H. Peng, J. He, Z. Sun, H. Xue, W. Guo, B. Liu, Y. Guo, H. Zhang, C. Zhao, Wire-arc directed energy deposition of oxide-modified H13 steel: Microstructural characterization and mechanical properties, Materials Science and Engineering: A 911 (2024) 146962.

[15] X. Du, Y. Wei, X. Liu, W. Zhao, R. Liu, Heat treatment routes and strengthening mechanism of H13 steel hybrid components produced by forging and additive manufacturing, Materials Science and Engineering: A 923 (2025) 147762.

[16] Q. Tan, Y. Yin, F. Wang, H. Chang, S. Liu, G. Liang, T. Wu, M.-X. Zhang, Rationalization of brittleness and anisotropic mechanical properties of H13 steel fabricated by selective laser melting, Scr. Mater. 214 (2022) 114645.

[17] A. Wang, J. Wang, F. Yang, T. Wen, M. Zhu, Y. Luo, S. Ji, H. Yang, Laser-powder bed fusion of Y_2O_3 nanoparticle modified CoCrNi matrix composites: Parameter optimization, microstructural evolution and strengthening mechanisms, Materials Science and Engineering: A 910 (2024) 146822.

[18] J. Majta, J.G. Lenard, M. Pietrzyk, A study of the effect of the thermomechanical history on the mechanical properties of a high niobium steel, Materials Science and Engineering: A 208(2) (1996) 249-259.

[19] J. Yan, H. Song, Y. Dong, W.-M. Quach, M. Yan, High strength (~2000 MPa) or highly ductile (~11%) additively manufactured H13 by tempering at different conditions, Materials Science and Engineering: A 773 (2020) 138845.

[20] T. Gladman, Precipitation hardening in metals, Mater. Sci. Technol. 15(1) (1999) 30-36.